

# Geophysical Research Letters

## RESEARCH LETTER

10.1029/2019GL082538

### Key Points:

- Nonideal electric field was observed in the separatrix region and inferred to be caused by gradient of the electron pressure tensor
- The nongyrotropic electron distribution and substantial energy dissipation were observed in the separatrix region
- Asymmetry between two sides of the current sheet was observed in the symmetric reconnection

### Correspondence to:

R. Wang and Q. Lu,  
rswan@ustc.edu.cn;  
qmlu@ustc.edu.cn

### Citation:

Yu, X., Wang, R., Lu, Q., Russell, C. T., & Wang, S. (2019). Nonideal electric field observed in the separatrix region of a magnetotail reconnection event. *Geophysical Research Letters*, *46*, 10,744–10,753. <https://doi.org/10.1029/2019GL082538>

Received 24 FEB 2019

Accepted 4 SEP 2019

Accepted article online 11 SEP 2019

Published online 16 OCT 2019

## Nonideal Electric Field Observed in the Separatrix Region of a Magnetotail Reconnection Event

Xiancai Yu<sup>1,2</sup> , Rongsheng Wang<sup>1,2</sup> , Quanming Lu<sup>1,2</sup> , Christopher T. Russell<sup>3</sup> , and Shui Wang<sup>1</sup>

<sup>1</sup>CAS Key Laboratory of Geospace Environment, Department of Geophysics and Planetary Science, University of Science and Technology of China, Hefei, China, <sup>2</sup>CAS Center for Excellence in Comparative Planetology, Hefei, China, <sup>3</sup>Earth Planetary and Space Sciences, University of California, Los Angeles, CA, USA

**Abstract** Based on the Magnetospheric Multiscale observations in the magnetotail, we present a complete crossing of the current sheet with ongoing magnetic reconnection. The field-aligned inflowing electrons were observed in both separatrix regions (SRs) and their energy extended up to several times of the thermal energy. Along the SR, a net parallel electrostatic potential was estimated and could be the reason for the inflowing electron streaming. In the northern SR, the electron frozen-in condition was violated and nonideal electric field was inferred to be caused by the gradient of the electron pressure tensor. The nongyrotropic electron distribution and significant energy dissipation were observed at the same region. The observations indicate that the inner electron diffusion region can extend along the separatrices or some electron-scale instability can be destabilized in the SR.

**Plain Language Summary** The microphysics in the separatrix region (SR) plays an important role for the energy conversion in reconnection. In this letter, we present nonideal electric field in the SR and the electron acceleration therein. These observations indicate that a significant part of energy conversion takes place in the SR during reconnection.

### 1. Introduction

Magnetic reconnection is a fundamental plasma process that converts magnetic field energy into plasma energy with reconfiguration of magnetic field topology (Lapenta et al., 2016; Petrukovich et al., 2016; Vasyliunas, 1975). In the collisionless plasma environments, the ideal frozen-in condition is broken in the reconnection diffusion region, and thus, the charged particles can be energized there. In the ion diffusion region, the ions are decoupled from the magnetic field, and the electrons are still frozen in the magnetic field. The separation of ions and electrons leads to the Hall current system in the vicinity of the ion diffusion region. As a result, the quadrupolar structure of the Hall magnetic field along the X-line direction and the Hall electric fields pointing toward the current sheet center at both sides are created in the vicinity of the reconnection diffusion region (Sonnerup, 1979; Uzdensky & Kulsrud, 2006; Wang et al., 2010). In the electron diffusion region where electrons are no longer coupled with the magnetic field, the electrons can be accelerated therein by the reconnection electric field originating from the electron pressure tensor (Hesse et al., 1999; Lu et al., 2013; Vasyliunas, 1975) and anomalous resistivity (Torbert et al., 2016).

As part of the Hall current system, the inflowing electrons are commonly observed to stream along the magnetic field in the separatrix region (SR; Nagai et al., 2001; Øieroset et al., 2001; Wang et al., 2010) and are associated with the density cavity (Mozer et al., 2002; Wang et al., 2012, 2013). In the SR, various instabilities and waves can be excited (Divin et al., 2012; Khotyaintsev et al., 2006; Lapenta et al., 2015), that is, the double layer (Wang et al., 2014), the electron holes (Cattell, 2005; Huang et al., 2014), lower hybrid waves (Graham et al., 2017), and whistler waves (Graham, Vaivads, et al., 2016). Recently, the energetic electrons with energies up to 120 keV were observed to be injected toward the X line in the SRs, at both ion outflow regions of one reconnection event (Lapenta et al., 2016; Wang et al., 2013, 2014). The parallel electric field directed away from the X-line was simultaneously detected in the SRs. However, it remains unclear how this parallel electric field was created and whether the parallel electric field was the unique reason for the high-energy electron beam. Egedal et al. (2012) proposed that an electrostatic potential should exist in a large region centered at the X-line and thereby trap as well as energize electrons therein. Although the

importance of the parallel electric field had been noticed in the SR (e.g., Egedal et al., 2010), the perpendicular electric field was rarely explored in the SR (Divin et al., 2012).

In this letter, we present a magnetic reconnection event encountered by Magnetospheric Multiscale (MMS) in the magnetotail. The four satellites of MMS crossed the reconnection earthward outflow region from the southern hemisphere to the northern hemisphere. The nonideal electric field perpendicular to the local magnetic field was observed in the northern SR and was inferred to be generated primarily by gradient of the electron pressure tensor.

## 2. Instrumentation

The MMS mission launched in March 2015 was designed to study the electron physics of magnetic reconnection with an unprecedentedly high-temporal resolution. The magnetic field data are obtained from the fluxgate magnetometers with a 7.8-ms time resolution in burst mode (Russell et al., 2016). The electric field data sampled at 8192/s is taken from the electric field double probe (Ergun et al., 2016; Lindqvist et al., 2014). The thermal particle data is obtained from the fast plasma investigation (Pollock et al., 2016), and the time resolutions for electrons and ions are 30 and 150 ms, respectively. In this letter, we mainly used the magnetic and electric field data, the plasma data from fast plasma investigation.

## 3. Observation and Analysis

During 09:43:10–09:43:40 UT on 19 June, the MMS spacecraft were located in the magnetotail at  $[-20.5, -2.5, 2.8]R_e$  in the Geocentric Solar Ecliptic (GSE) coordinate system, and the separation between the four spacecraft was less than 20 km. During this time interval, MMS passed through the neutral sheet from the south hemisphere to the north hemisphere. In order to investigate this crossing, the minimum variance analysis (MVA; Sonnerup & Scheible, 1998) was performed to the magnetic field at MMS1 during this interval to obtain local boundary coordinates,  $L=[0.9658, 0.2341, 0.1112]$ ,  $M=[-0.2473, 0.7039, 0.6659]$ , and  $N=[0.0776, -0.6706, 0.7377]$  relative to GSE coordinates. Because of the small separation, the measurements at the four satellites were more or less the same for the whole interval except in some localized regions, that is, the north edge of the diffusion region. Therefore, we used the data from MMS3 in this letter. Unless otherwise stated, the local boundary coordinates were used.

Figure 1 shows the complete crossing of the magnetotail current sheet, characterized by the reversal of  $B_L$  from  $\sim -15$  nT to  $\sim 15$  nT. The plasma beta  $\beta$ , calculated by  $P_{\text{plasma}}/P_{\text{mag}}$  (Baumjohann et al., 1989), peaked at  $B_L \approx 0$ . It was larger than 1 in the both hemispheres and up to 100 at the current sheet center, consistent with the crossing of the plasma sheet. As the spacecraft traversed the plasma sheet, the earthward bulk ion flows (up to 150 km/s  $\sim 0.16V_A$ ,  $V_A$  is the Alfvén speed based on the electron density  $N = 0.12 \text{ cm}^{-3}$  in the inflow region) were observed in the center, and the magnetic field component  $B_M$  varied from negative in the southern hemisphere to positive in the northern hemisphere. Thus, the observations of the ion bulk flows and the magnetic field were well consistent with a crossing of the reconnection ion diffusion region earthward of the X-line, as shown in Figure 1j. The earthward electron bulk flows were much stronger than the ion flows, and were close to 2,500 km/s,  $\sim 2.7V_A$  during 09:43:22.2–09:43:26.6 UT. In the two boundary regions of the earthward electron flows, the tailward electron flows were observed at  $\sim 09:43:20$  and  $\sim 09:43:27$  UT, and the duration was about 1 s, much shorter than the earthward electron flows of  $\sim 4$  s. The type of electron flows and the resultant electron currents are in good agreement with the Hall electron current system (Deng & Mastsumoto, 2001; Lu et al., 2010; Nagai et al., 2001; Øieroset et al., 2001). The earthward electron flows correspond to the reconnection electron outflows, while the tailward flows are the inflowing electrons. The electron inflow speed approached 2,000 km/s in the southern SR. In the northern SR, the electron inflow speed reached 4,000 km/s ( $\sim 4.2V_A$ ; 09:43:26.6–09:43:27.6 UT), larger than the outflow speed ( $\leq 2,500$  km/s), to our knowledge, which has never been observed by the spacecraft before. In simulations (Divin et al., 2012; Egedal et al., 2015; Hesse et al., 2018), the acceleration of the inflowing electrons was evident in the separatrix. Divin et al. (2012) found the inflowing speed in the SR was as large as  $30V_A$ , much stronger than the outflow speed.

In this crossing, the electric field was the most intense in the  $N$  direction, and  $E_N$  was positive in the southern hemisphere and negative in the northern hemisphere, consistent with the Hall electric field, except for at the

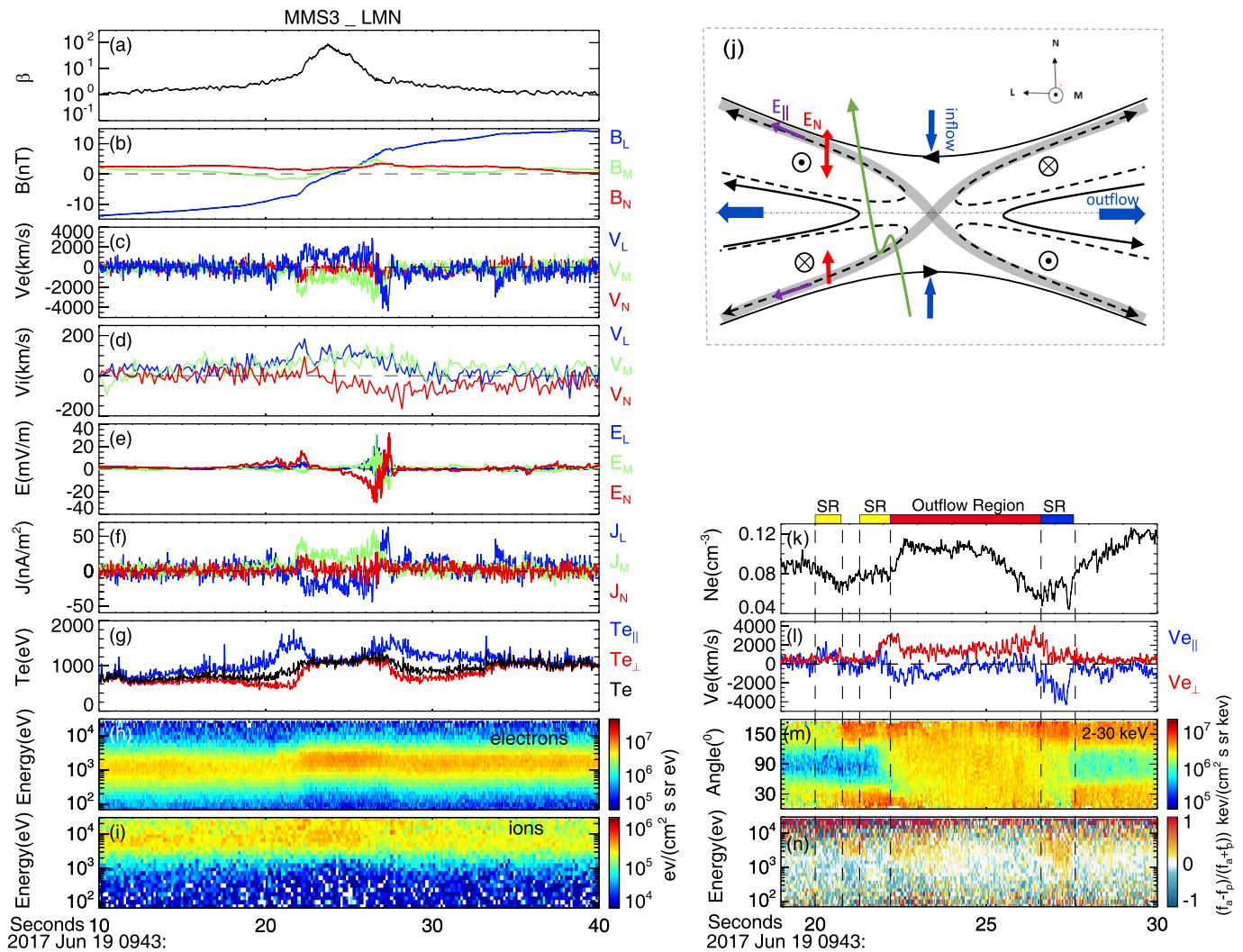


**Figure 1.** (a) Plasma  $\beta$ . (b)  $B$ . (c–d)  $V_e$  and  $V_i$ . (e)  $E$ . (f) Current density  $J = en(V_i - V_e)$ . (g)  $T_e$  and  $T_{e||}$ ,  $T_{e\perp}$ . (h–i) Electron and ion energy spectrum. (j) A schematic illustrator of reconnection diffusion region. The green curve represents the Magnetospheric Multiscale trajectory. The gray shadow area denotes the region near the separatrix. (k–n) The color bars at the top represent the different regions, in which the yellow (blue) bar is the southern (northern) separatrix region (SR), corresponding to the electron inflowing, and the red bar is the outflow region. (k)  $N_e$  derived from the spacecraft potential. (l)  $V_{e||}$ ,  $V_{e\perp}$ . (m) Electron pitch angle distributions (2–30 keV). (n) Electron field-aligned anisotropic distribution  $(f_a - f_p)/(f_a + f_p)$ .

northward edge (09:43:27.2–09:43:27.6 UT) where  $E_N$  reversed to be positive again (Figure 1e). This abnormal electric field was inconsistent with the previous observations of the Hall electric field in the reconnection diffusion region. Simultaneously, the large amplitude fluctuations were detected in all three components. The instabilities developing in the direction perpendicular to magnetic field direction were investigated recently by numerical simulations (Divin et al., 2012). A new electron jet instability developed in the perpendicular direction and produced the bipolar perpendicular electric field. This simulation result is very similar to the observation here.

The hotter ion and electron populations were observed in the plasma sheet, and the electron temperature showed a special profile. The parallel temperature  $T_{e||}$  was significantly enhanced but depressed at the center. The perpendicular temperature  $T_{e\perp}$  had a high level at the center of the plasma sheet. As a result,  $T_{e||}$  was comparable to  $T_{e\perp}$  at the center while larger than  $T_{e\perp}$  away from the center. This electron temperature profile is similar to that in the electron current sheet reported recently (Wang et al., 2018). The total electron temperature  $T_e$  was higher in the northern hemisphere than in the southern hemisphere (Figure 1g). The reason for this asymmetry between two hemispheres will be discussed later. The ion flows in the  $M$  direction were

toward the dusk side, while the electron flows were primarily toward the dawn side, indicating that the crossing was close to the electron diffusion region (EDR; e.g., Wang et al., 2017).

Based on the analysis above, we conclude that the spacecraft crossed a reconnection ion diffusion region earthward of the EDR. The normal direction and speed of the current sheet were estimated by the timing analysis (Schwartz, 1998), which was performed to the  $B_L = 0$  points. The speed was about 98.5 km/s along the  $[0.379, 0.299, -0.876]$  direction in the  $LMN$  coordinates. According to the duration of  $\sim 7.6$  s ( $\sim 09:43:20.0$ – $09:43:27.6$  UT), the half thickness of the current sheet was estimated to be 749 km  $\sim 1.4d_i$ , where  $d_i = 537$  km. The boundary regions with the inflowing electrons were named as the SR here. The duration for the north SR was 1 s, and thus, the thickness was roughly 100 km  $\sim 0.18d_i$ . In the southern hemisphere, MMS entered the SR at  $\sim 09:43:20.0$  UT and left at  $\sim 09:43:20.8$  UT. Shortly thereafter, MMS reentered the SR at  $\sim 09:43:21.3$  UT. So the duration of the southern separatrix was about 0.8 s, and the thickness was about 80 km  $\sim 0.15d_i$ . The repeated crossings of the SR region might be due to the rapid motion of the current sheet.

In both SRs, the inflowing electrons were primarily along the magnetic field, and parallel (antiparallel to) to the magnetic field in the south (north) SR (Figure 11). The inflowing electrons coincided with the density cavity derived from the spacecraft potential (Andriopoulou et al., 2018), which was in agreement with the previous observations (Khotyaintsev et al., 2006; Wang et al., 2013, 2014). The pitch angle distribution of the electrons at energies from 2 to 30 keV was displayed in Figure 1m. The electron differential energy fluxes were significantly enhanced along the magnetic field directions ( $\sim 0^\circ$  and/or  $\sim 180^\circ$ ) and were depleted around the perpendicular directions ( $\sim 90^\circ$ ) before 09:43:22.2 UT and after 09:43:26.6 UT. In the center of the current layer between 09:43:22.2 and 09:43:26.6 UT, the electron distribution was nearly isotropic. Figure 1n shows electron field-aligned anisotropy defined as  $(f_a - f_p)/(f_a + f_p)$  where  $f_a$  and  $f_p$  are the energy fluxes antiparallel and parallel to magnetic field, respectively. It is evident that there was an electron streaming antiparallel to magnetic field (red) within the cavity in the northern SR, and the energy of the electron streaming was from hundreds of eV to more than 10 keV. The electron field-aligned anisotropy data were complicated in the south hemisphere due to the repeated crossings of the SR.

In the south SR, the energy of the inflowing electrons was no less than 6 keV. The energy of the inflowing electrons extended to 10 keV in the northern SR. Therefore, we conclude that the electrons were significantly accelerated in the SRs. In order to determine the acceleration mechanism(s) and the reason for the abnormal electric field in the northern SR, we analyzed the electric field data in details. The strong fluctuations of the parallel electric field were found around both SRs, as the blue trace in Figure 2b. The most intense  $E_{\parallel}$  fluctuations were observed at 09:43:26.5–09:43:27.8 UT, that is, the northern SR. It can be found that the average parallel electric field  $E_{\text{ave}}$  (red trace, by averaging every 50 points of the parallel electric field data) was positive in the northern SR and mainly negative in the southern SR, illustrated in Figure 1j as the purple arrows. Although the parallel electric field in the SR was in agreement with the inflowing electron flows, the electric field errors were comparable to the parallel electric field.

In order to confirm the existence of the parallel electric field in the SR, we estimated the electrostatic potential by Liouville's theorem (Egedal et al., 2013; Graham et al., 2014; Eriksson et al., 2018). In the Figures 2g and 2h, we chose the inflow electron distributions (the pink lines) from both sides of the CS (at 09:43:10 UT and 09:43:39 UT, not shown in the figure) with isotropic distribution. The net potential was estimated to be 1,050 V along the magnetic field in the northern SR (Figure 2h) and was about 500 V in the southern SR (Figure 2g). This result further supports our conclusion that the parallel electric field was indeed along the SR. The derived parallel electrostatic potential in the SR could be the reason for the preacceleration of the inflowing electrons.

The measured perpendicular electric field at the barycenter of the four satellites is displayed in Figures 2d–2f. According to the generalized Ohm's law shown below (Torbert et al., 2016; Vasyliunas, 1975), the electron convection term  $-(\mathbf{V}_e \times \mathbf{B})$ , the electron inertia term  $-\frac{\nabla \cdot (m_e n_e \mathbf{V}_e \mathbf{V}_e) + \partial m_e n_e \mathbf{V}_e / \partial t}{en_e}$ , and the gradient term of the electron pressure  $-\nabla \cdot \mathbf{P} / en_e$  except for the resistivity term  $\eta \mathbf{J}$  are shown.

$$\mathbf{E} + \mathbf{V}_e \times \mathbf{B} = \eta \mathbf{J} - \frac{\nabla \cdot \mathbf{P}}{en_e} - \frac{\nabla \cdot (m_e n_e \mathbf{V}_e \mathbf{V}_e) + \partial m_e n_e \mathbf{V}_e / \partial t}{en_e}$$

$\eta$  is the anomalous resistivity maybe due to wave-particle interaction. Figures 2d–2f show the perpendicular

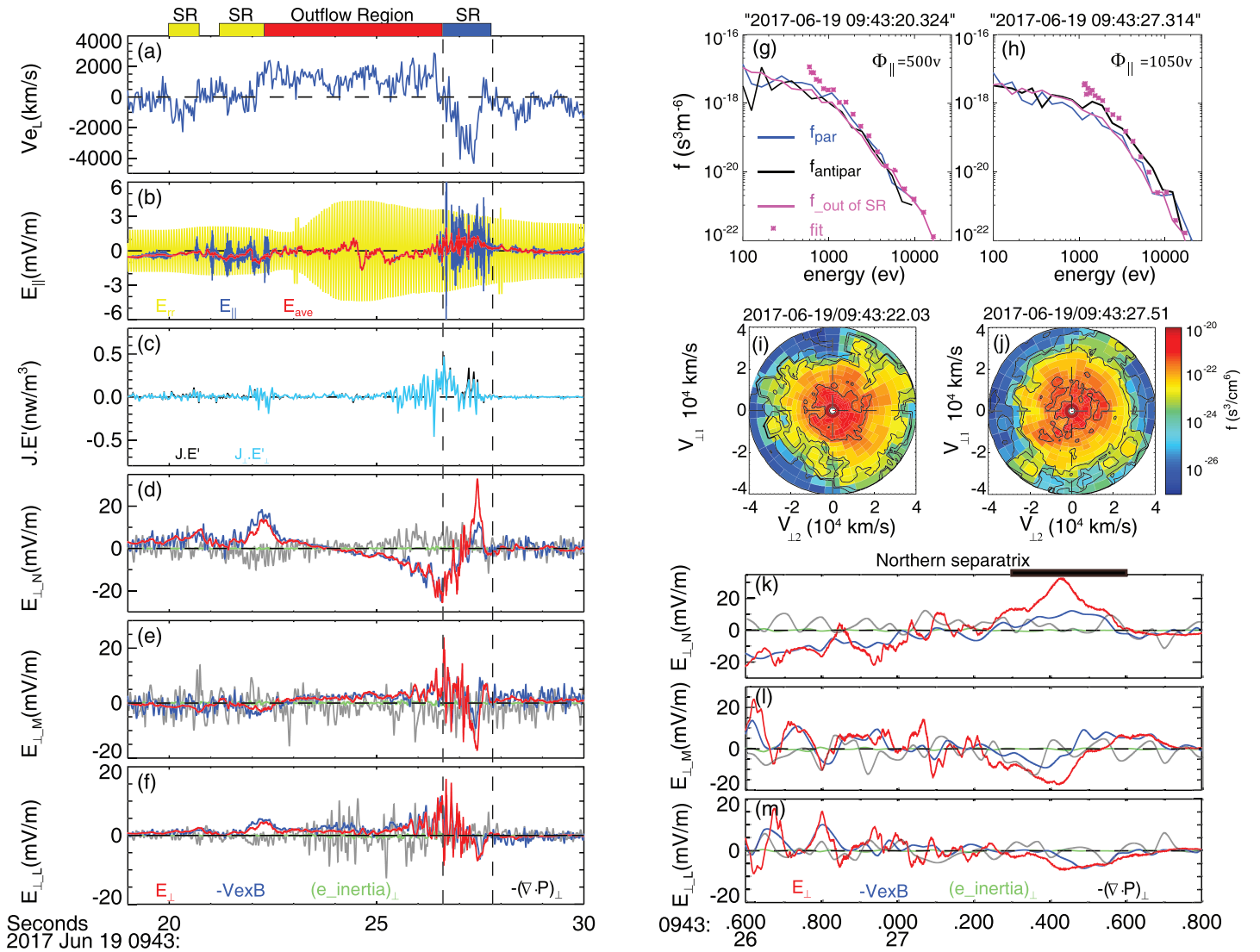


**Figure 2.** (a)  $V_{eL}$ . (b) The parallel (blue) and the average parallel (red) electric field, with the errors in yellow. (c)  $\mathbf{J} \cdot \mathbf{E}'$  and  $\mathbf{J}_{\perp} \cdot \mathbf{E}'_{\perp}$ . (d–f) The terms of Ohm's law in the three component:  $\mathbf{E}_{\perp}$  (red),  $-(\mathbf{V}_e \times \mathbf{B})$  (blue),  $-\left(\frac{\nabla \cdot (m_e n_e \mathbf{V}_e \mathbf{V}_e) + \partial m_e n_e \mathbf{V}_e / \partial t}{en_e}\right)_{\perp}$  (green), and  $-\left(\frac{\nabla \cdot \mathbf{P}}{en_e}\right)_{\perp}$  (gray). (g–h) Electron phase-space density in the southern and northern separatrix, respectively. The inflow distribution (pink lines), the Liouville mapping of the inflow distribution accelerated by  $\Phi_{\parallel}$  (pink asterisks), and the local parallel (blue) and antiparallel (black) electron distributions. (i–j) Electron velocity distribution functions at times indicated, in which  $\mathbf{V}_{\perp 1} = (\mathbf{b} \times \mathbf{v})$ ,  $\mathbf{V}_{\perp 2} = (\mathbf{v} \times \mathbf{b}) \times \mathbf{b}$ . (k–m) The terms of Ohm's law in three components for the northern separatrix region (SR).

components of the measured electric field (red traces), the electron convection term (blue traces), the electron inertia term (green traces), and the gradient of the electron pressure tensor term (gray traces). The measured electric field was in good agreement with the electron convection term, except in both SRs, especially the northern SR. Thus, the electron frozen-in condition kept very well in the crossing except in the northern SR.

The electric field data in the northern SR was enlarged in Figures 2k–2m. The deviation between the measured electric field (red) and the electron convection term (blue) was significant during 09:43:27.2–09:43:27.6 UT, especially in the  $N$  and  $M$  directions (Figures 2k and 2l). The electron inertia term (green) was always close to zero, meaning a negligible role for the deviation. The gradient of electron pressure tensor (gray) fluctuated largely. So it is unclear how this nonideal electric field was created.

The electron distribution function in the perpendicular plane was analyzed during the whole crossing. In both southern and northern SRs, the nongyrotropic electron distribution was observed. Figures 2i and 2j

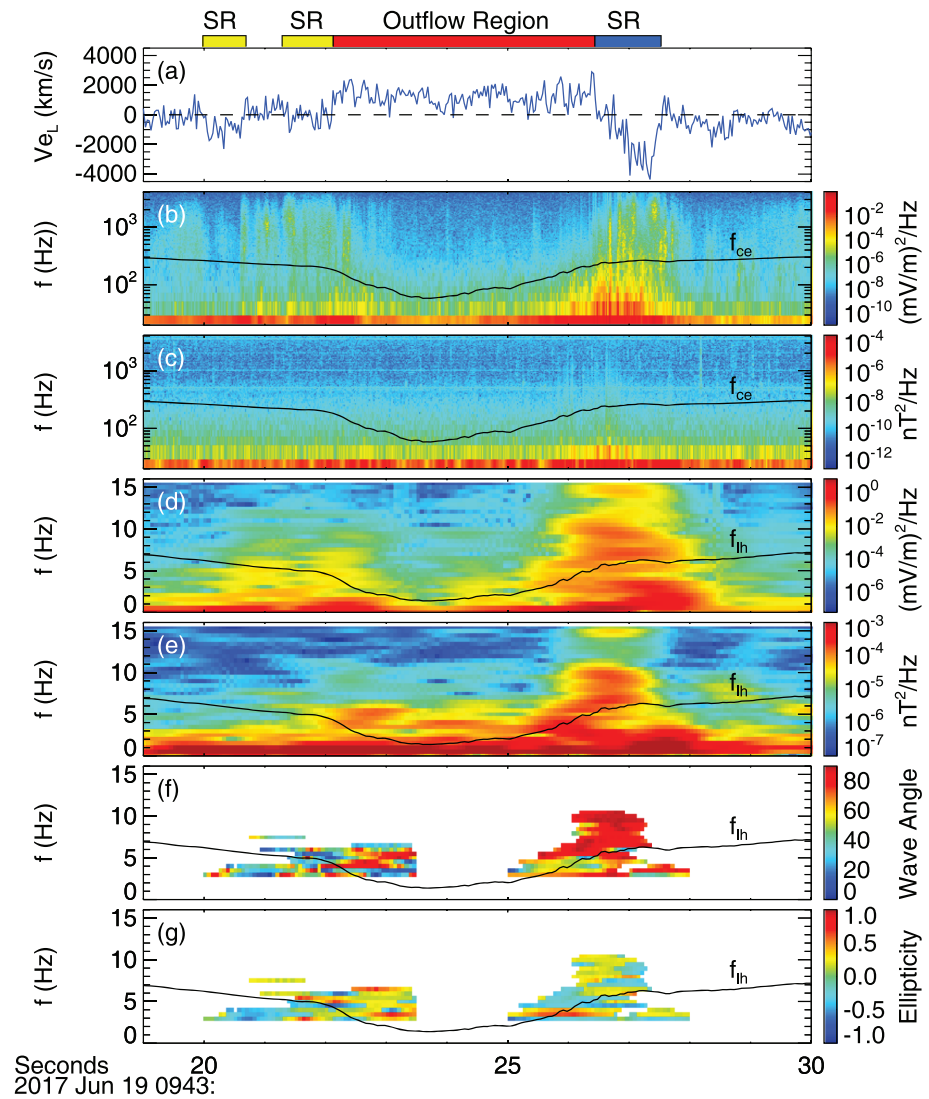


**Figure 3.** Wave analysis using fast Fourier transforms from MMS3. (a)  $V_{eL}$ . (b–c) The power spectrum of  $E$  and  $B$  in the high frequency band. (d–g) The power spectrum of  $E$  and  $B$ , wave angle, and ellipticity in the low-frequency band. The black curves are the electron plasma frequency  $f_{ce}$  and the lower hybrid frequency  $f_{lh}$  in (b)–(c) and (d)–(g), respectively. SR = separatrix region.

show one example of the electron distribution functions in the southern and northern SR, respectively. The electron fluxes in the right sector were higher than those in the left sector. The nongyrotropic distribution was observed during 09:43:21.95–09:43:22.2 UT in the southern SR. In the northern SR, the nongyrotropic distribution was coincided with the nonideal electric field, as the black bar at the top of Figure 2k. The energy dissipation  $\mathbf{J} \cdot \mathbf{E}$  was mainly enhanced in both SRs and dominated by its perpendicular component (Figure 2c). It was very weak in the southern SR ( $\sim 0.1 \text{ nW/m}^3$ ) and became significant in the northern SR ( $\sim 0.4 \text{ nW/m}^3$ ).

Figure 3 shows the wave analysis during 09:43:19–09:43:30 UT. The wave normal angle and ellipticity were obtained from the fast Fourier transforms (Samson & Olson, 1980). The broadband electrostatic emission up to the electron plasma frequency was substantial in both the SRs (Figure 3b), closely related to the large amplitude fluctuations of the parallel electric field. At the lower frequencies, the electromagnetic emissions were observed around the lower hybrid frequency and were confined in the SRs (Figures 3d and 3e). The wave power was larger in the northern SR than in the southern SR. In the northern SR, the wave normal angle was  $\sim 90^\circ$ , and the ellipticity was near zero, which was consistent with the lower hybrid drift waves.

In the southern SR, the wave normal angle and the ellipticity were uncertain. Since the gradient of the plasma density and magnetic field was strong in the SR (Figures 1b and 1k), the lower hybrid waves were likely excited there (Krall & Liewer, 1971; Retinò et al., 2006).

#### 4. Discussion and Summary

In this letter, we report a crossing by MMS of the ion diffusion region in the magnetotail. According to the Hall electric and magnetic field signature, reconnection ion outflows, and the Hall electron current system, we conclude that the spacecraft passed through the ion diffusion region earthward of a reconnection X-line from the southern hemisphere to the northern hemisphere. Magnetic reconnection in the magnetotail is generally regarded as symmetric reconnection (e.g., Mozer et al., 2008), that is, the plasma and the magnetic field are equal at both sides of the current sheet. In our event, although the magnitude of the reconnecting magnetic field and the plasma density were nearly equal on both sides, the electron inflowing speed, the electric field intensity and the fluctuations of electric and magnetic field on both sides were significantly different. The electron inflowing speed in the southern SR was much weaker than that in the northern SR. Moreover, the Hall electric field was less than 15 mV/m in the southern hemisphere and close to 30 mV/m in the northern hemisphere. The electric and magnetic field fluctuations in the southern SR were weaker than those in the northern SR also.

This kind of asymmetric reconnection ion diffusion region was observed by all of the four satellites. One potential explanation for this asymmetry was the spatial variation. If so, it is still unclear how this asymmetry was created. The ambient guide field  $B_g$  was about 1 nT, and the ratio between  $B_g$  and the magnetic field magnitude in the lobe region was about  $\sim 0.07$ . So this is a weak component reconnection. According to the simulations, the reconnection results would not be altered significantly while the ratio was smaller than 0.3 (Fu et al., 2006; Pritchett, 2001). Alternatively, this asymmetry was due to the temporal evolution of the ion diffusion region. As the spacecraft crossed the ion diffusion region, the reconnection rate increased and therefore the asymmetry between two sides of the ion diffusion region was produced. The average speed of the inflowing ions ( $V_{iN}$ ) was about 4 km/s in the southern hemisphere, and it became  $\sim 45$  km/s in the northern hemisphere. Thus, the reconnection rate was  $\sim 0.004$ , while the spacecraft was in the southern hemisphere and increased to 0.05 as the spacecraft entered into the northern hemisphere. Because the reconnection rate increased, the electrons were heated to the higher temperature in the northern hemisphere. The electron temperature enhancement was just observed at the region with the intense gradient of the magnetic field and the lower-hybrid drift waves. The curvature drift (Le Roux et al., 2015) and lower-hybrid waves could be the reason for the electron energization. Based on the analysis, it seems that the observed asymmetry between two hemispheres was caused by the temporal evolution of the reconnection itself.

The field-aligned inflowing electrons were observed at both southern and northern SRs. In the southern SR, the inflowing speed was comparable to the electron outflowing speed and became larger than the outflowing speed in the northern SR. Moreover, the energy of these inflowing electrons extended up to 10 keV. Thus, the inflowing electrons were accelerated before they entered into the inner electron diffusion region. Since the electron pitch angle data for the higher energy are unavailable in this event, we cannot confirm whether the inflowing electrons can be accelerated to higher energy as reported previously (Lapenta et al., 2016; Wang et al., 2013, 2014).

In the northern SR, the electron frozen-in condition was violated evidently. To our knowledge, the electron frozen-in condition is only broken in the so-called electron diffusion region based on the theory (Bessho et al., 2014; Hesse et al., 2014; Le et al., 2013; Lu et al., 2013; Wang et al., 2001) and in situ measurements (Burch et al., 2016; Wang et al., 2018), and it has never been observed in the SR. In order to figure out the reason, we calculated the electron convection term, the gradient term of the electron pressure, the electron inertial term, and anomalous resistivity term of the generalized Ohm's law in the narrow non-ideal electric field layer. The electron convection term could account for about half of the measured electron field. The inertial term was close to zero. The pressure tensor gradient term fluctuated in this narrow layer too. Thus, we cannot exclude the role of the pressure tensor gradient term. Because the lower-hybrid waves were very strong in the northern SR, we estimated the anomalous resistivity term from the interaction of the waves around the lower-hybrid frequency with the particles (Coroniti, 1985) and it was less than 0.005 mV/m therein (not shown). Thus, the anomalous resistivity term would play a negligible role in this event,

different from the reference of Torbert et al. (2016) where the authors suggested that the resistive term played a role for the electric field in the inner EDR.

The nongyrotropic distribution was extensively studied recently by the MMS data and was generally observed in the proximity of the inner electron diffusion region (Burch et al., 2016; Tang et al., 2019). Here, we found that nongyrotropic distribution was formed in the SR as well. According to the simulations of Scudder and Daughton (2008) and Swisdak (2016), the electron agyrotropy peaked at the separatrix and the X-point. Namely, the electron agyrotropy extended from the X-point to the SR (e.g., Hesse et al., 2011). This explains why the nongyrotropic electron distribution was observed in the SR in our event. Because the electron distribution was nongyrotropic in the SR, the divergence of the electron pressure tensor should be significant, although it cannot be derived accurately from the estimated pressure tensor term due to the strong fluctuation. In addition, the gradient of the density from the spacecraft potential was substantial (Figure 1k) and directed away from the cavity center, and mainly perpendicular to the local magnetic field. Thus, we suggest that the gradient of electron pressure plays an important role for the nonideal electron field, analogous to the situation in the electron diffusion region (Lu et al., 2013; Torbert et al., 2016).

On the other hand, Divin et al. (2012) simulated the instability of the electron flows along the separatrix and predicted the generation of bipolar electric field in one perpendicular direction. In the numerical simulations (Divin et al., 2012), the electron-scale dynamic jets were created and evolved rapidly along the separatrix. The simulation results can explain our observations, for example, the high speed inflowing jet, the intense electric field fluctuations. If a satellite was inserted in the simulations, the asymmetry between two hemispheres could have been observed as well. The subion scale processes were observed in the ion diffusion region and could energize the electrons during asymmetric reconnection at the magnetopause (e.g., Graham, Khotyaintsev, et al., 2016). Thus, this kind of the subion-scale processes could be common in both symmetric and asymmetric reconnection and played an important for the heating and acceleration of the electrons.

In summary, we investigated the electric and magnetic structures, electron distribution, and wave feature during the crossing of the reconnection ion diffusion region from the southern hemisphere to the northern hemisphere in the magnetotail. The evident asymmetric distribution, including the Hall electric field and fluctuation intensity, the inflowing electron speed, and electron temperature, between two sides of the current sheet were observed and attributed to the time evolution of the reconnection itself. The field-aligned inflowing electrons with a few to 10 keV were observed in both SRs. It indicates that the inflowing electrons had been preaccelerated before they entered the electron diffusion region. The net parallel electric field directed away from the X-line in the SR was the one possible reason for this acceleration. Furthermore, the electron frozen-in condition was broken in some localized regions of the SR, and the nonideal electric field was related to the gradient of the electron pressure.

#### Acknowledgments

R. Wang appreciate the discussion and suggestions from Yuri Khotyaintsev at Swedish Institute of Space Physics. All the MMS data used in this work are available at the MMS data center (<https://lasp.colorado.edu/mms/sdc/>). This work is supported by the National Science Foundation of China (NSFC) grants (41527804, 41674143, 41922030, and 41421063) and by the National Basic Research Program of China (2013CBA01503).

#### References

- Andriopoulou, M., Nakamura, R., Wellenzohn, S., Torkar, K., Baumjohann, W., Torbert, R. B., et al. (2018). Plasma density estimates from spacecraft potential using MMS observations in the dayside magnetosphere. *Journal of Geophysical Research: Space Physics*, *123*, 2620–2629. <https://doi.org/10.1002/2017JA025086>
- Baumjohann, W., Paschmann, G., & Cattell, C. A. (1989). Average plasma properties in the central plasma sheet. *Journal of Geophysical Research*, *94*(A6), 6597–6606. <https://doi.org/10.1029/JA094iA06p06597>
- Bessho, N., Chen, L.-J., Shuster, J. R., & Wang, S. (2014). Electron distribution functions in the electron diffusion region of magnetic reconnection: Physics behind the fine structures. *Geophysical Research Letters*, *41*, 8688–8695. <https://doi.org/10.1002/2014GL062034>
- Burch, J. L., Torbert, R. B., Phan, T. D., Chen, L. J., Moore, T. E., Ergun, R. E., et al. (2016). Electron-scale measurements of magnetic reconnection in space. *Science*, *352*(6290), aaf2939. <https://doi.org/10.1126/science.aaf2939>
- Cattell, C. (2005). Cluster observations of electron holes in association with magnetotail reconnection and comparison to simulations. *Journal of Geophysical Research*, *110*, A01211. <https://doi.org/10.1029/2004JA010519>
- Coroniti, F. V. (1985). Space plasma turbulent dissipation: Reality or myth? *Space Science Reviews*, *42*(399), 1985.
- Deng, X. H., & Mastumoto, H. (2001). Rapid magnetic reconnection in the Earth's magnetosphere mediated by whistler waves. *Nature*, *410*(6828), 557–560. <https://doi.org/10.1038/35069018>
- Divin, A., Lapenta, G., Markidis, S., Newman, D. L., & Goldman, M. V. (2012). Numerical simulations of separatrix instabilities in collisionless magnetic reconnection. *Physics of Plasmas*, *19*(4), 042110. <https://doi.org/10.1063/1.3698621>
- Egedal, J., Daughton, W., & Le, A. (2012). Large-scale electron acceleration by parallel electric fields during magnetic reconnection. *Nature Physics*, *8*(4), 321–324. <https://doi.org/10.1038/nphys2249>
- Egedal, J., Daughton, W., Le, A., & Borg, A. L. (2015). Double layer electric fields aiding the production of energetic flat-top distributions and superthermal electrons within magnetic reconnection exhausts. *Physics of Plasmas*, *22*(10), 101208. <https://doi.org/10.1063/1.4933055>
- Egedal, J., Le, A., & Daughton, W. (2013). A review of pressure anisotropy caused by electron trapping in collisionless plasma, and its implications for magnetic reconnection. *Physics of Plasmas*, *20*(6), 061201. <https://doi.org/10.1063/1.4811092>

- Egedal, J., Lê, A., Zhu, Y., Daughton, W., Øieroset, M., Phan, T., et al. (2010). Cause of super-thermal electron heating during magnetotail reconnection. *Geophysical Research Letters*, *37*, L10102. <https://doi.org/10.1029/2010GL043487>
- Ergun, R. E., Tucker, S., Westfall, J., Goodrich, K. A., Malaspina, D. M., Summers, D., et al. (2016). The axial double probe and fields signal processing for the MMS mission. *Space Science Reviews*, *199*(1–4), 167–188. <https://doi.org/10.1007/s11214-014-0115-x>
- Eriksson, E., Vaivads, A., Graham, D. B., Divin, A., Khotyaintsev, Y. V., Yordanova, E., et al. (2018). Electron energization at a reconnecting magnetosheath current sheet. *Geophysical Research Letters*, *45*, 8081–8090. <https://doi.org/10.1029/2018GL078660>
- Fu, X. R., Lu, Q. M., & Wang, S. (2006). The process of electron acceleration during collisionless magnetic reconnection. *Physics of Plasmas*, *13*(1). <https://doi.org/10.1063/1.2164808>
- Graham, D. B., Khotyaintsev, Y. V., Norgren, C., Vaivads, A., André, M., Lindqvist, P.-A., et al. (2016). Electron currents and heating in the ion diffusion region of asymmetric reconnection. *Geophysical Research Letters*, *43*, 4691–4700. <https://doi.org/10.1002/2016GL068613>
- Graham, D. B., Khotyaintsev, Y. V., Norgren, C., Vaivads, A., André, M., Toledo-Redondo, S., et al. (2017). Lower hybrid waves in the ion diffusion and Magnetospheric inflow regions. *Journal of Geophysical Research: Space Physics*, *122*, 517–533. <https://doi.org/10.1002/2016JA023572>
- Graham, D. B., Khotyaintsev, Y. V., Vaivads, A., André, M., & Fazakerley, A. N. (2014). Electron dynamics in the diffusion region of an asymmetric magnetic reconnection. *Physical Review Letters*, *112*(21). <https://doi.org/10.1103/PhysRevLett.112.215004>
- Graham, D. B., Vaivads, A., Khotyaintsev, Y. V., & André, M. (2016). Whistler emission in the separatrix regions of asymmetric magnetic reconnection. *Journal of Geophysical Research: Space Physics*, *121*, 1934–1954. <https://doi.org/10.1002/2015JA021239>
- Hesse, M., Aunai, N., Sibeck, D., & Birn, J. (2014). On the electron diffusion region in planar, asymmetric, systems. *Geophysical Research Letters*, *41*, 8673–8680. <https://doi.org/10.1002/2014GL061586>
- Hesse, M., Neukirch, T., Schindler, K., Kuznetsova, M., & Zenitani, S. (2011). The diffusion region in collisionless magnetic reconnection. *Space Science Reviews*, *160*(1–4), 3–23. <https://doi.org/10.1007/s11214-010-9740-1>
- Hesse, M., Norgren, C., Tenfjord, P., Burch, J. L., Liu, Y. H., Chen, L. J., et al. (2018). On the role of separatrix instabilities in heating the reconnection outflow region. *Physics of Plasmas*, *25*(12). <https://doi.org/10.1063/1.5054100>
- Hesse, M., Schindler, K., Birn, J., & Kuznetsova, M. (1999). The diffusion region in collisionless magnetic reconnection. *Physics of Plasmas*, *6*(5), 1781–1795. <https://doi.org/10.1063/1.873436>
- Huang, C., Lu, Q., Wang, P., Wu, M., & Wang, S. (2014). Characteristics of electron holes generated in the separatrix region during antiparallel magnetic reconnection. *Journal of Geophysical Research: Space Physics*, *119*, 6445–6454. <https://doi.org/10.1002/2014JA019991>
- Khotyaintsev, Y. V., Vaivads, A., Retinò, A., André, M., Owen, C. J., & Nilsson, H. (2006). Formation of inner structure of a reconnection separatrix region. *Physical Review Letters*, *97*(20), 205003. <https://doi.org/10.1103/PhysRevLett.97.205003>
- Krall, N. A., & Liewer, P. C. (1971). Low-frequency instabilities in magnetic pulses. *Physical Review A*, *4*(5), 2094–2103. <https://doi.org/10.1103/PhysRevA.4.2094>
- Lapenta, G., Markidis, S., Divin, A., Newman, D., & Goldman, M. (2015). Separatrices: The crux of reconnection. *Journal of Plasma Physics*, *81*(1). <https://doi.org/10.1017/S0022377814000944>
- Lapenta, G., Wang, R., & Cazzola, E. (2016). Reconnection separatrix: Simulations and spacecraft measurements. In W. Gonzalez, & E. Parker (Eds.), *Magnetic reconnection: Concepts and applications* (pp. 315–344). Switz: Springer. [https://doi.org/10.1007/978-3-319-26432-5\\_8](https://doi.org/10.1007/978-3-319-26432-5_8)
- Le, A., Egedal, J., Ohia, O., Daughton, W., Karimabadi, H., & Lukin, V. S. (2013). Regimes of the electron diffusion region in magnetic reconnection. *Physical Review Letters*, *110*(13), 135004. <https://doi.org/10.1103/PhysRevLett.110.135004>
- Le Roux, J., Zank, G., Webb, G., & Khabarova, O. (2015). A kinetic transport theory for particle acceleration and transport in regions of multiple contracting and reconnecting inertial-scale flux ropes. *The Astrophysical Journal*, *801*(2), 112. <https://doi.org/10.1088/0004-637X/801/2/112>
- Lindqvist, P.-A., Olsson, G., Torbert, R. B., King, B., Granoff, M., Rau, D., et al. (2014). The spin-plane double probe electric field instrument for MMS. *Space Science Reviews*, *199*(1–4), 137–165. <https://doi.org/10.1007/s11214-014-0116-9>
- Lu, Q. M., Huang, C., Xie, J. L., Wang, R. S., Wu, M. Y., Vaivads, A., & Wang, S. (2010). Features of separatrix regions in magnetic reconnection: Comparison of 2-D particle-in-cell simulations and Cluster observations. *Journal of Geophysical Research*, *115*, A11208. <https://doi.org/10.1029/2010JA015713>
- Lu, Q. M., San, L., Can, H., Mingyu, W., & Wang, S. (2013). Self-reinforcing process of the reconnection electric field in the electron diffusion region and onset of collisionless magnetic reconnection. *Plasma Physics and Controlled Fusion*, *55*(8). <https://doi.org/10.1088/0741-3335/55/8/085019>
- Mozer, F., Pritchett, P., Bonnell, J., Sundkvist, D., & Chang, M. (2008). Observations and simulations of asymmetric magnetic field reconnection. *Journal of Geophysical Research*, *113*, A00C03. <https://doi.org/10.1029/2008JA013535>
- Mozer, F. S., Bale, S. D., & Phan, T. D. (2002). Evidence of diffusion regions at a sub-solar magnetopause crossing. *Physical Review Letters*, *89*(1), 015002. <https://doi.org/10.1103/PhysRevLett.89.015002>
- Nagai, T., Shinohara, I., Fujimoto, M., Hoshino, M., Saito, Y., Machida, S., & Mukai, T. (2001). Geotail observations of the Hall current system: Evidence of magnetic reconnection in the magnetotail. *Journal of Geophysical Research*, *106*(A11), 25929–25949. <https://doi.org/10.1029/2001JA900038>
- Øieroset, M., Phan, T. D., Fujimoto, M., Lin, R. P., & Lepping, R. P. (2001). In situ detection of collisionless reconnection in the Earth's magnetotail. *Nature*, *412*(6845), 414–417. <https://doi.org/10.1038/35086520>
- Petrukovich, A., Artemyev, A., & Nakamura, R. (2016). Magnetotail reconnection. In W. Gonzalez & E. Parker (Eds.), *Magnetic reconnection: Concepts and applications* (pp. 277–314). Switzerland: Springer International. [https://doi.org/10.1007/978-3-319-26432-5\\_7](https://doi.org/10.1007/978-3-319-26432-5_7)
- Pollock, C., Moore, T., Jacques, A., Burch, J., Gliese, U., Saito, Y., et al. (2016). Fast plasma investigation for Magnetospheric Multiscale. *Space Science Reviews*, *199*(1–4), 331–406. <https://doi.org/10.1007/s11214-016-0245-4>
- Pritchett, P. L. (2001). Geospace environment modeling magnetic reconnection challenge: Simulations with a full particle electromagnetic code. *Journal of Geophysical Research*, *106*(A3), 3783–3798. <https://doi.org/10.1029/1999JA001006>
- Retinò, A., Vaivads, A., André, M., Sahraoui, F., Khotyaintsev, Y., Pickett, J. S., et al. (2006). Structure of the separatrix region close to a magnetic reconnection X-line: Cluster observations. *Geophysical Research Letters*, *33*, L06101. <https://doi.org/10.1029/2005GL024650>
- Russell, C. T., Anderson, B. J., Baumjohann, W., Bromund, K. R., Dearborn, D., Fischer, D., et al. (2016). The Magnetospheric Multiscale magnetometers. *Space Science Reviews*, *199*(1–4), 189–256. <https://doi.org/10.1007/s11214-014-0057-3>
- Samson, J. C., & Olson, J. V. (1980). Some comments on the descriptions of the polarization states of waves. *Geophysical Journal of the Royal Astronomical Society*, *61*(1), 115–129. <https://doi.org/10.1111/j.1365-246X.1980.tb04308.x>

- Schwartz, S. J. (1998). Shock and discontinuity normals, Mach numbers, and related parameters. In G. Paschmann & P. W. Daly (Eds.), *Analysis methods for multi spacecraft data* (pp. 249–267). Bern Switzerland: Eur. Space Agency.
- Scudder, J., & Daughton, W. (2008). Illuminating electron diffusion regions of collisionless magnetic reconnection using electron agyrotropy. *Journal of Geophysical Research*, *113*, A06222. <https://doi.org/10.1029/2008JA013035>
- Sonnerup, B. U. Ö. (1979). Magnetic field reconnection. In L. T. Lanzerotti, C. F. Kennel, & E. N. Parker (Eds.), *Solar system plasma physics* (pp. 45–108). New York: North-Holland.
- Sonnerup, B. U. Ö., & Scheible, M. (1998). Minimum and maximum variance analysis. In G. Paschmann & P. W. Daly (Eds.), *Analysis methods for multi spacecraft data* (pp. 185–215). Bern Switzerland: Eur. Space Agency.
- Swisdak, M. (2016). Quantifying gyrotropy in magnetic reconnection. *Geophysical Research Letters*, *43*, 43–49. <https://doi.org/10.1002/2015GL066980>
- Tang, B.-B., Li, W. Y., Graham, D. B., Rager, A. C., Wang, C., Khotyaintsev, Y. V., et al. (2019). Crescent-shaped electron distributions at the non-reconnecting magnetopause: Magnetospheric Multiscale observations. *Geophysical Research Letters*, *46*, 3024–3032. <https://doi.org/10.1029/2019GL082231>
- Torbert, R. B., Burch, J. L., Giles, B. L., Gershman, D., Pollock, C. J., Dorelli, J., et al. (2016). Estimates of terms in Ohm's law during an encounter with an electron diffusion region. *Geophysical Research Letters*, *43*, 5918–5925. <https://doi.org/10.1002/2016GL069553>
- Uzdensky, D. A., & Kulsrud, R. M. (2006). Physical origin of the quadrupole out-of-plane magnetic field in Hall-magnetohydrodynamic reconnection. *Physics of Plasmas*, *13*(6), 062305. <https://doi.org/10.1063/1.2209627>
- Vasyliunas, V. M. (1975). Theoretical models of magnetic field line merging. *Reviews of Geophysics*, *13*(1), 303–336. <https://doi.org/10.1029/RG013i001p00303>
- Wang, R., du, A., Nakamura, R., Lu, Q., Khotyaintsev, Y. V., Volwerk, M., et al. (2013). Observation of multiple sub-cavities adjacent to single separatrix. *Geophysical Research Letters*, *40*, 2511–2517. <https://doi.org/10.1002/grl.50537>
- Wang, R., Lu, Q., Khotyaintsev, Y. V., Volwerk, M., du, A., Nakamura, R., et al. (2014). Observation of double layer in the separatrix region during magnetic reconnection. *Geophysical Research Letters*, *41*, 4851–4858. <https://doi.org/10.1002/2014GL061157>
- Wang, R., Lu, Q., Nakamura, R., Baumjohann, W., Huang, C., Russell, C. T., et al. (2018). An electron-scale current sheet without bursty reconnection signatures observed in the near-Earth tail. *Geophysical Research Letters*, *45*, 4542–4549. <https://doi.org/10.1002/2017GL076330>
- Wang, R., Lu, Q. M., Huang, C., & Wang, S. (2010). Multispacecraft observation of electron pitch angle distributions in magnetotail reconnection. *Journal of Geophysical Research*, *115*, A01209. <https://doi.org/10.1029/2009JA014553>
- Wang, R., Nakamura, R., Lu, Q., Baumjohann, W., Ergun, R. E., Burch, J. L., et al. (2017). Electron-scale quadrants of the Hall magnetic field observed by the Magnetospheric Multiscale spacecraft during asymmetric reconnection. *Physical Review Letters*, *118*(17). <https://doi.org/10.1103/PhysRevLett.118.175101>
- Wang, R., Nakamura, R., Lu, Q., du, A., Zhang, T., Baumjohann, W., et al. (2012). Asymmetry in the current sheet and secondary magnetic flux ropes during guide field magnetic reconnection. *Journal of Geophysical Research*, *117*, A07223. <https://doi.org/10.1029/2011JA017384>
- Wang, X. G., Bhattacharjee, A., & Ma, Z. W. (2001). Scaling of collisionless forced reconnection. *Physical Review Letters*, *87*(26). <https://doi.org/10.1103/PhysRevLett.87.265003>